Author(s): Andreeova, K. & Pulkkinen, Tuija I. & Juusola, L. & Palmroth, M. & Santolik, O.

Title: Propagation of a shock-related disturbance in the Earth's magnetosphere

Year: 2011

Version: Final published version

Please cite the original version:

Andreeova, K. & Pulkkinen, Tuija I. & Juusola, L. & Palmroth, M. & Santolik, O.. 2011. Propagation of a shock-related disturbance in the Earth's magnetosphere. Journal of geophysical research, Vol. 116, nro A01213. P. 10. 0148-0227 (printed). DOI: 10.1029/2010JA015908.

Propagation of a shock-related disturbance in the Earth's magnetosphere

K. Andreeova,[1] T. I. Pulkkinen,[2] L. Juusola,[2] M. Palmroth,[2] and O. Santolík[3,4]

Received 7 July 2010; revised 8 September 2010; accepted 1 November 2010; published 27 January 2011.

[1] The Grand Unified Magnetosphere-Ionosphere Coupling Simulation, version 4, magnetohydrodynamic simulation of the interplanetary shock event on 9 November 2002 is used to determine the shock-associated disturbance propagation characteristics inside the Earth's magnetosphere. Interaction of an interplanetary fast forward shock with the magnetopause caused a shock-related disturbance inside the magnetosphere that propagated at a speed significantly higher than that in the solar wind or magnetosheath. The propagation direction of the disturbance was calculated from the Rankine-Hugoniot conditions, velocity and magnetic coplanarity, and minimum variance analysis and is shown to vary in different regions of the magnetosphere. Furthermore, the impulse disturbance wave mode changes as the plasma and field conditions change inside the magnetosphere. These results bring important new information about the propagation processes that is not directly obtainable from point measurements made by (even several) spacecraft. On the other hand, comparison of ionospheric observations from the IMAGE magnetometer chain with geosynchronous data allow us to also interpret the double step structure observed at dayside geosynchronous orbit, which is below the simulation resolution. This combination provides us with quite a complete view on shock propagation inside the magnetosphere.

Citation: Andreeova, K., T. I. Pulkkinen, L. Juusola, M. Palmroth, and O. Santolík (2011), Propagation of a shock-related disturbance in the Earth's magnetosphere, *J. Geophys. Res.*, *116*, A01213, doi:10.1029/2010JA015908.

1. Introduction

[2] Sudden increases in the solar wind dynamic pressure, such as interplanetary shocks, cause compression of the magnetosphere and earthward motion of the magnetopause. At the same time, the magnetopause current is intensified. The motion and intensification of the current is recorded at the Earth's surface as a sudden increase in the geomagnetic field intensity. This feature is known as a sudden impulse, or sudden commencement [*Le et al.*, 1998; *Le and Russell*, 1998; *Zhuang et al.*, 1981].

[3] Interplanetary shocks can be divided into four groups according to the associated changes in the solar wind plasma and interplanetary magnetic field (IMF) [*Burlaga*, 1971]: fast forward, fast reverse, slow forward, and slow reverse shocks. These are mainly driven by two sources, coronal mass ejections (CME) and corotating interaction regions (CIR). This study concentrates on fast forward shock (FFS) events, which propagate earthward from the sun with speed of about 50–200 km/s in the reference frame of the ambient plasma [*Berdichevsky et al.*, 2000].

[4] Interaction of the fast forward shocks with the Earth's bow shock and magnetopause has been studied by several authors using gas dynamic and magnetohydrodynamic (MHD) models or Rankine-Hugoniot conditions [*Spreiter and Stahara*, 1994; *Grib et al.*, 1979; *Grib*, 1982; *Zhuang et al.*, 1981]. There are different approaches to study how the IP shock propagates through the magnetosphere, whether it is by the IP shock driven at the magnetopause or a wave launched by the interaction of the magnetopause with the IP shock, which is already discussed by *Huttunen et al.* [2005] and *Collier et al.* [1998]. After interaction with the fast forward shock, the bow shock starts to move earthward [*Šafránková et al.*, 2007]. Three new discontinuities appear downstream from the bow shock in addition to the FFS: a forward slow expansion wave, a contact discontinuity, and a reverse slow shock [*Koval et al.*, 2005, 2006b; *Samsonov et al.*, 2006]. Even if the shock surface in the solar wind is curved at larger scales, on the scale size of the Earth's magnetosphere it is sufficient to assume that the shock front is planar [*Szabo et al.*, 2001]. In the magnetosheath, the shock front becomes curved especially near the flanks of the magnetotail [*Koval et al.*, 2005, 2006b; *Samsonov et al.*, 2006] and decelerated to speeds in the range from about one third to about a quarter of the original shock speed [*Koval et al.*, 2005; *Villante et al.*, 2004]. A time delay from the first interaction of the shock with the bow shock to the observation of the disturbance on the ground has been estimated to be approximately about 5 min [*Villante et al.*, 2004].

[1]Department of Physics, University of Helsinki, Helsinki, Finland.
[2]Finnish Meteorological Institute, Helsinki, Finland.
[3]Institute of Atmospheric Physics AS CR, Prague, Czech Republic.
[4]Also at Faculty of Mathematics and Physics, Charles University, Prague, Czech Republic.

0148-0227/11/2010JA015908

[5] The fast mode wave

$$v_F = \sqrt{\frac{1}{2}\left[\left(v_A^2 + c_S^2\right) + \left\{\left(v_A^2 + c_S^2\right)^2 - 4v_A^2 c_S^2 \cos^2\theta\right\}^{\frac{1}{2}}\right]} \quad (1)$$

is higher in the Earth's magnetosphere than in the solar wind near Earth orbit. A FFS propagating with shock front almost perpendicular to the Sun-Earth line causes a sudden increase in the solar wind dynamic pressure, speed, and magnetic field. When the FFS reaches the magnetopause, the earthward motion of the boundary produces different types of waves propagating within the magnetosphere: *Tamao* [1964] found isotropic compressional hydrodynamic waves generated at the magnetopause, propagating inward into the magnetosphere at speeds higher than the local Alfvén wave speed. *Wilken et al.* [1982] estimated the propagation speeds to be about 600 km/s in the radial direction from geostationary orbit to ground, and about 910 km/s in the azimuthal direction in the equatorial plane. Finally, *Nopper et al.* [1982] estimated an impulse disturbance speed about 1500 km/s at geostationary orbit.

[6] Recently, *Juusola et al.* [2010] referred to the topic of ionospheric signatures of the arrival of a pressure pulse at the magnetopause. The main source of ground magnetic disturbances at high latitudes are the ionospheric electrojet currents, which can be modeled as spherical surface current density $\mathbf{J}(\theta, \phi)$, divided into divergence-free (df) and curl-free (cf) components.

[7] Assuming that there is no significant potential drop along the magnetic field lines, the Hall component of the current, flowing antiparallel to the ionospheric $|\mathbf{E} \times \mathbf{B}|$ drift is then mapping to the magnetosphere.

[8] This paper describes observation and simulation results of the interaction of a fast forward shock with the Earth's bow shock, magnetopause and magnetosphere. Section 2 describes used methods and global MHD simulation Grand Unified Magnetosphere-Ionosphere Coupling Simulation, version 4 (GUMICS-4). Section 3 introduces the observations, section 4 discusses the disturbance direction and speed, while section 5 concentrates on the wave modes. Section 6 introduces the ionospheric observations and their relation to high-altitude magnetic field signatures. Section 7 concludes the paper with discussion.

2. Methodology

2.1. Minimum Variance Analysis, Coplanarity, and Rankine-Hugoniot Methods

[9] For the study of the disturbance propagation we need to determine the disturbance normals and speeds. There are a variety of approaches using observations from a single spacecraft or simultaneous data from multiple spacecraft. Some methods can only provide the shock normal. The velocity of the disturbance is usually derived from the mass flux conservation law:

$$V_s = \frac{\Delta[\rho \mathbf{V}]}{\Delta\rho} \cdot \mathbf{n} \quad (2)$$

where V_s is disturbance speed, ρ is plasma density, and n is normal vector, and the notation Δ [] refers to difference across the shock.

[10] Variance analysis [*Paschmann et al.*, 1988] is based on searching for minimum change in one component of the magnetic field from single spacecraft data. A single spacecraft passing through a 1-D surface observes variations in the magnetic field. Since $\nabla \cdot \mathbf{B} = 0$, the normal component of the magnetic field must be constant. Thus, the minimum variance analysis looks for a unique direction along which the product of $\mathbf{B} \cdot \mathbf{n}$ is zero. This direction corresponds to the normal direction. This method can fail for pure MHD shock solutions or if the three eigenvalues of the variance matrix are not sufficiently distinct.

[11] The normal to a planar surface can be also determined using the coplanarity theorem. Magnetic (MC) [*Lepping and Argentiero*, 1971] and velocity (VC) [*Abraham-Shrauner*, 1972] coplanarity conditions can be written as follows:

$$n_{MC} = \pm\frac{(\mathbf{B_d} \times \mathbf{B_u}) \times \Delta[\mathbf{B}]}{|(\mathbf{B_d} \times \mathbf{B_u}) \times \Delta[\mathbf{B}]|} \quad (3)$$

$$n_{VC} = \pm\frac{\mathbf{V_d} - \mathbf{V_u}}{|\mathbf{V_d} - \mathbf{V_u}|} \quad (4)$$

where suffixes d and u in the equations denote downstream and upstream of the disturbance, in the sense of direction of the flow. The dominant change in velocity is usually along the shock normal, especially when the plasma Mach number ranges from moderate to high.

[12] Magnetic coplanarity determination fails for $\theta_{Bn} = 0°$ or 90°. It is also possible to combine both normal determinations in finding the solution.

[13] Rankine-Hugoniot (RH) conditions can be written as the following set of equations [*Szabo*, 1994]:

$$\Delta[G_n] \equiv \Delta[\rho(V_n - V_S)] = 0$$

$$\Delta[B_n] \equiv \Delta[\mathbf{B} \cdot \hat{n}] = 0$$

$$\Delta[\mathbf{S_t}] \equiv \Delta\left[\rho(V_n - V_S)\mathbf{V_t} - \frac{B_n}{\mu_0}\mathbf{B_t}\right] = 0$$

$$\Delta[\mathbf{E_t}] \equiv \Delta[(\hat{n} \times \mathbf{V_t})B_n - (V_n - V_S)(\hat{n} \times \mathbf{B_t})] = 0$$

$$\Delta[S_n] \equiv \Delta\left[P + \frac{{B_t}^2}{2\mu_0} + \rho(V_n - V_S)^2\right] = 0$$

$$\Delta[\varepsilon] \equiv \Delta\left[\rho(V_n - V_S)\left(\frac{(\mathbf{V} - V_S\hat{n})^2}{2} + \frac{\gamma}{\gamma - 1}\frac{P}{\rho} + \frac{B^2}{\mu_0\rho}\right) - \frac{B_n(\mathbf{V} - V_S\hat{n}) \cdot \mathbf{B}}{\mu_0}\right] = 0$$

where V_S is the shock speed along the normal, γ is the ratio of specific heats, μ_0 is the vacuum permeability, ρ is plasma density, $P = nkT$ is the total scalar isotropic thermal pressure, and $\hat{n}$ is the shock normal unit vector. The subscripts n and t refer to the normal and tangential components of the above quantities. The variables G_n, B_n, $\mathbf{S_t}$, $\mathbf{E_t}$, S_n, and ε denote the conserved quantities across the shock: the mass flux, normal magnetic field, tangential momentum flux, tangential electric field, normal momentum flux, and energy flux. The notation Δ [] refers to the difference across the shock.

[14] As magnetic coplanarity method does not work for $\theta_{Bn} = 0°$ or 90°, and minimum variance analysis fails for

pure MHD shock solutions or if the variance direction is degenerated, the best method for our calculations using GUMICS-4 simulation results were obtained by using the minimum variance analysis. Velocity coplanarity method provides good results at high Mach numbers and for θ_{Bn} near 0° or 90° for which magnetic stresses are unimportant.

[15] It is important to note that analyzing simulation results where the field and plasma values are available at every grid point is very different from using observations from single spacecraft or even a cluster of several satellites. This means that methods that are optimal for observational analysis are not necessarily the best to use in the case of simulations.

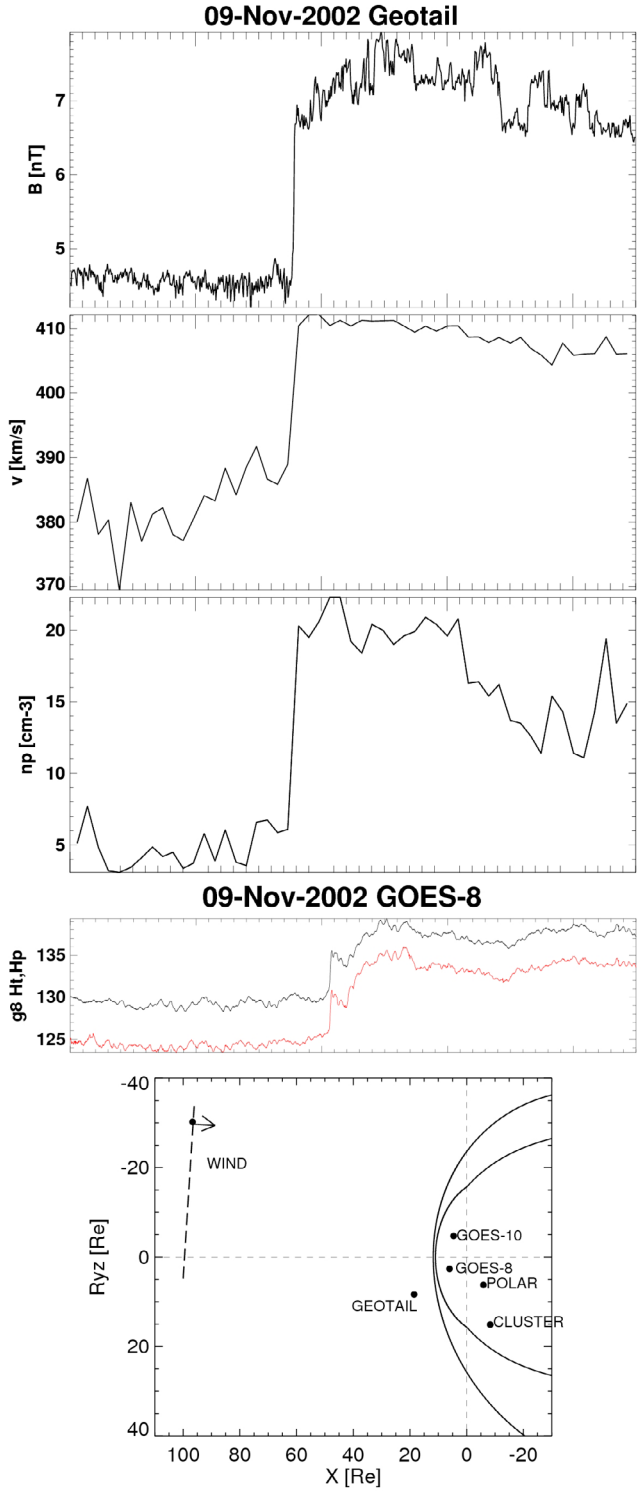

Figure 1. Event FFS observed by Geotail upstream the Earth's bow shock: the first panel shows total magnetic field, the second panel shows total solar wind speed, and the third panel shows solar wind plasma density. The fourth panel shows observation of the GOES 8 high-resolution magnetic field data in local S/C coordinated (H_t is magnitude, and H_p is northward component (in red)). The fifth panel shows positions of given satellites for the event. The dashed line indicates the fast forward shock front. The *Jeřáb et al.* [2005] and *Petrinec and Russell* [1996] models were used to determine the bow shock and magnetopause positions before the shock arrival. R_{yz} denotes the distance from the X axis, distinguishing the dawn/dusk sides (sign of Y), $R_{yz} = sign(y) \cdot \sqrt{y^2 + z^2}$.

2.2. GUMICS-4 Simulation

[16] The GUMICS-4 global magnetohydrodynamic (MHD) simulation solves the ideal MHD equations to provide the self-consistent temporal and spatial evolution of the plasma dynamics in the magnetosphere and the solar wind [*Janhunen*, 1996]. The fully conservative MHD equations are solved in a simulation box extending from 32 R_E upstream of the Earth to −224 R_E in the tailward direction and ±64 R_E in the directions perpendicular to the Sun-Earth line. The equations are solved in the geocentric solar ecliptic (GSE) coordinates. The inner boundary of the MHD domain is a spherical shell with a radius of 3.7 R_E, which maps along the dipole field to about 60° latitude. The MHD grid is adaptive in a sense that the grid is automatically refined to a minimum cell size of 0.25 R_E whenever the code detects large spatial gradients. Solar wind density, temperature, velocity, and magnetic field are given as boundary conditions along the sunward boundary while supersonic outflow conditions are applied on the other boundaries of the simulation box. It is assumed that B_X in the interplanetary field is constant to ensure that the field at the sunward edge of the simulation box is divergenceless.

[17] For the events studied in this paper, the simulation was run with a maximum resolution of 0.25 R_E, and the data were stored at 1 min intervals. It is assumed that B_X in the interplanetary field is zero.

3. Event Introduction

[18] We examine a FFS event that occurred on 9 November 2002 (for detailed observations, see *Andréeová and Přech* [2007]), in Figure 1. The FFS was observed by Wind at 1724 UT, and had a shock normal vector $(-0.99, 0.15, -0.05)_{RH}$ in the GSE coordinates, as deduced using the Wind data and the Rankine-Hugoniot method. The interplanetary magnetic field was Parker-spiral-like. As B_z was dominant and positive, northward IMF conditions prevailed. FFS was observed first by ACE satellite, then by Wind satellite, followed by Geotail satellite upstream the Earth's bow shock. Figure 1 shows observation by Geotail satellite in the solar wind and GOES 8 satellite in the dayside

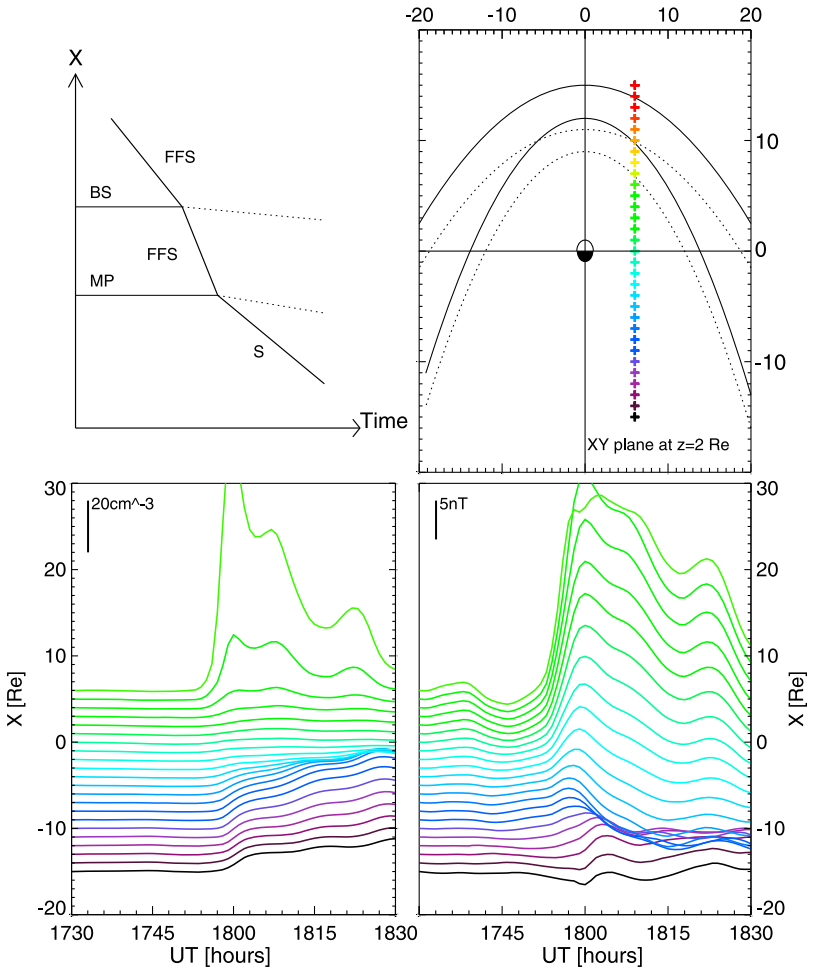

Figure 2. GUMICS-4 global MHD simulation results: (top left) Schematic illustration of the propagation along the Sun-Earth line. The impulse disturbance speed is proportional to the steepness of the curve in the *X*-time plane. Interaction of the fast forward shock (FFS) with the bow shock (BS) results in a modified bow shock (dashed line) and a slower FFS, whose interaction with the magnetopause (MP) results in an impulse disturbance (S) propagating inward. (top right) Noon-midnight meridian view of the magnetosphere. North is to the right. The bow shock and magnetopause locations (solid lines) are shown together with the locations modified by the shock interaction (dashed lines). The colored crosses indicate locations from which simulation results are shown in Figure 2 (bottom). Color coding shows red in the solar wind, green in the dayside, and blue to black colors in the nightside. (bottom left) Plasma density from the simulation. The scale is indicated by the vertical bar in the top left corner. The scale on the left indicates position in *X*; each curve starts from the *X* distance given by the scale. (bottom right) Magnetic field intensity with the dipole field subtracted from the simulation in a format similar to Figure 2 (bottom left).

magnetosphere. The fifth panel in Figure 1 denotes positions of given satellites for the event.

[19] For this event we found a very steep initial part of the magnetic field compression in the GOES high-resolution data, with practically the same duration as the shock fronts in the solar wind (about 10 s) as observed by Geotail satellite (Figure 1), followed by a small decrease of magnetic field magnitude, and a second much slower increase. This double step-like structure lasted all together about 5 min.

4. Analysis of Disturbance Direction and Speed

[20] Observational analysis of the fast forward shock propagation shows that disturbance speed in the Earth's magnetosphere is higher than the original shock speed in the solar wind [*Andréeová and Přech*, 2007; *Andréeová et al.*, 2008], and MHD simulation of the event shows similar results. The evolution of the speed along the Sun-Earth line is schematically illustrated in Figure 2 (top left). The magnetopause starts to move earthward with a speed of about 30 km/s after interaction with the FFS. At the same time, a disturbance is launched at the magnetopause, propagating inward through the Earth's magnetosphere. Below, we will use the velocity coplanarity method to calculate the disturbance propagation direction inside the magnetosphere. Also the disturbance speed is computed.

[21] Figure 2 shows the disturbance propagation through the Earth's magnetosphere along a line, which is parallel to

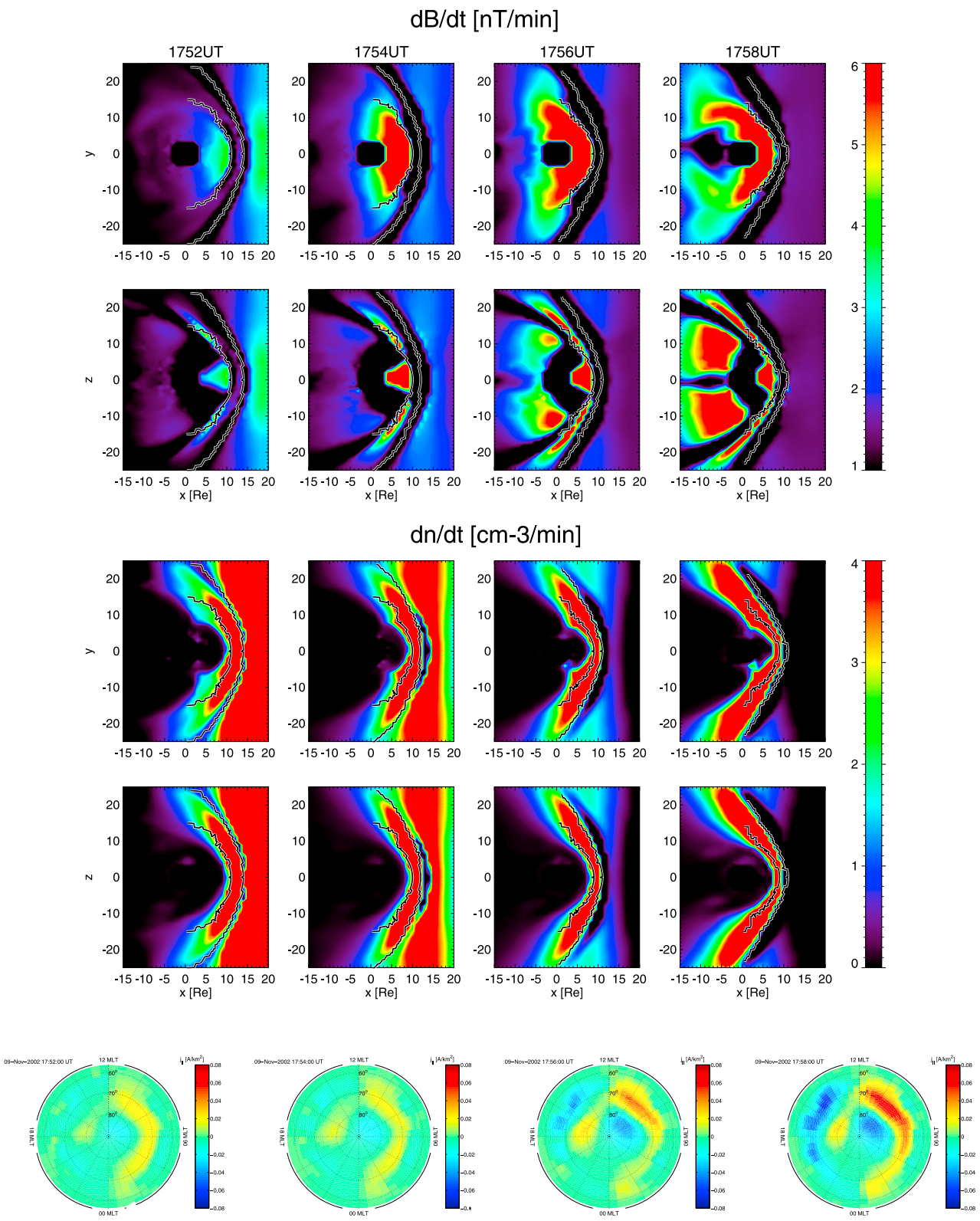

Figure 3. Interaction of the fast forward shock with the magnetosphere in the GUMICS-4 global MHD simulation. The first and second rows show the magnetic field temporal changes ($\Delta B/\Delta t$), while the third and fourth rows show the plasma density temporal changes ($\Delta n/\Delta t$) color coded, with color bars below the four rows. Each row shows four times, 1752, 1754, 1756, and 1758 UT; times are shown at the top of each column. The first and third rows show the magnetospheric equatorial plane, while the second and fourth rows show the noon-midnight meridian plane. The fifth row shows the field-aligned currents in the Northern Hemisphere ionosphere.

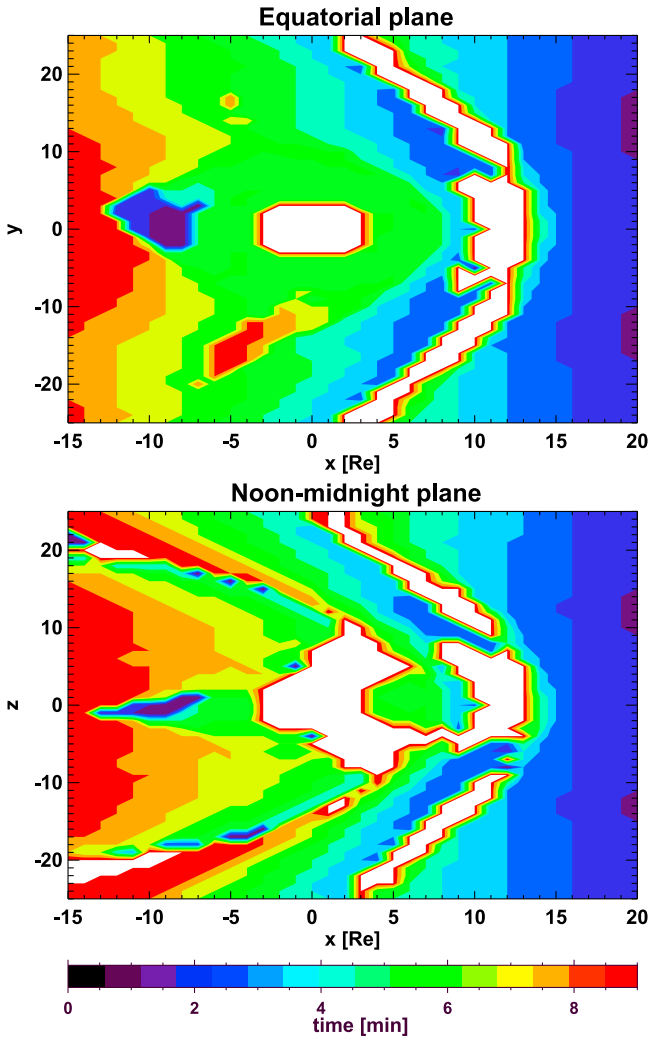

Figure 4. Shock/disturbance front propagation in time from 1751 (dark violet color) till 1759 UT (red color) in (top) the equatorial cross section and (bottom) the noon-midnight meridian plane. Color coding shows 1 min time step.

the Sun-Earth line and intersects the Polar satellite location in the nightside. Comparison of these model results with Polar observations are discussed by *Andréeová et al.* [2008]. Figure 2 (bottom) shows the density and magnetic field compression propagation along that line. The multiple curves show the density and magnetic field values at an X distance given by the scale on the left at the start of the time series at 1730 UT. Thus, the green to blue to purple colors give the density and magnetic field at distances ranging from 6 R_E on the dayside to −15 R_E on the nightside. It is clearly seen that the highest compression in both quantities was recorded in the dayside magnetosphere (values from the solar wind and magnetosheath are not shown for clarity). The compression of the magnetic field gradually decreases approximately out to −10 R_E, after which the structure of the disturbance is changed rather to fluctuations. The plasma density compression is also larger on the dayside, close to the Earth the compression almost disappears. However, the plasma density compression reappears in the nightside. Such behavior is better illustrated in Figure 3, which shows the response propagation in two different cross sections, noon-midnight meridian and equatorial planes.

[22] The first and second rows of Figure 3 show the time derivative of the magnetic field in the equatorial and noon-midnight meridian planes, respectively. The third and fourth rows in Figure 3 show similar derivatives for the plasma density. The time differences were computed using two data files saved 1 min apart. The first and second rows in Figure 3 show the two ways of propagation inside the magnetosphere: The first row in Figure 3 shows how the disturbance propagates through the dayside plasma sheet and turns around the inner tail toward the midnight sector plasma sheet. This direction change explains why the compression reappears in the nightside in Figure 2. The second row in Figure 3 shows how the disturbance propagates very fast along the magnetopause and somewhat slower through the lobe regions, again showing that the inner tail is the last region to record the disturbance. The third and fourth rows in Figure 3 show how temporal changes of plasma density, computed similarly to the field changes, evolve in time. Disturbance propagates especially fast tailward along the magnetopause, while changes are much smaller in the propagation inside the magnetosphere. Although difficult to see in this color scale chosen to highlight the initial changes, a small enhancement of the plasma density inside the magnetosphere was associated with the impulse disturbance passage. The fifth row in Figure 3 shows the field-aligned currents and the formation of a four-cell convection pattern. In this case, the northward IMF and slightly positive B_y caused a small asymmetry in the four-cell convection pattern.

5. Analysis of the Disturbance Mode in the Magnetosphere

[23] Expanding the one-dimensional view provided in Figure 2 we calculate the position of the disturbance at different times in the full three-dimensional space inside the magnetosphere, using minimum variance analysis. Figure 4 illustrates the shock/disturbance location during 1751–1759 UT, in 1 min time steps, as it propagates from the solar wind through the Earth's magnetosphere. Each color, representing a 1 min time step, shows where the disturbance was observed in the solar wind, magnetosheath and magnetosphere at that particular time. The inner part of the simulation (ionosphere), bow shock, magnetopause, and locations where no changes in plasma or magnetic field parameters were observed are shown white. The interplanetary shock propagated perpendicular to the Sun-Earth line with constant shock speed in the solar wind, which is shown in the illustration as a vertical front during the first time steps in the solar wind. After interaction with bow shock and later with the magnetopause, the shock/disturbance front is deformed and propagates with different speeds in different locations. Figure 4 clearly depicts how the disturbance front is carried by the magnetic field directly tailward through the lobes and around the Earth in the equatorial plane, in concert with the time series in Figure 3.

[24] Figure 5 shows the shock/disturbance speed (color coding) and propagation direction (arrows) in the equatorial plane (Figure 5, left) and in the noon-midnight meridian

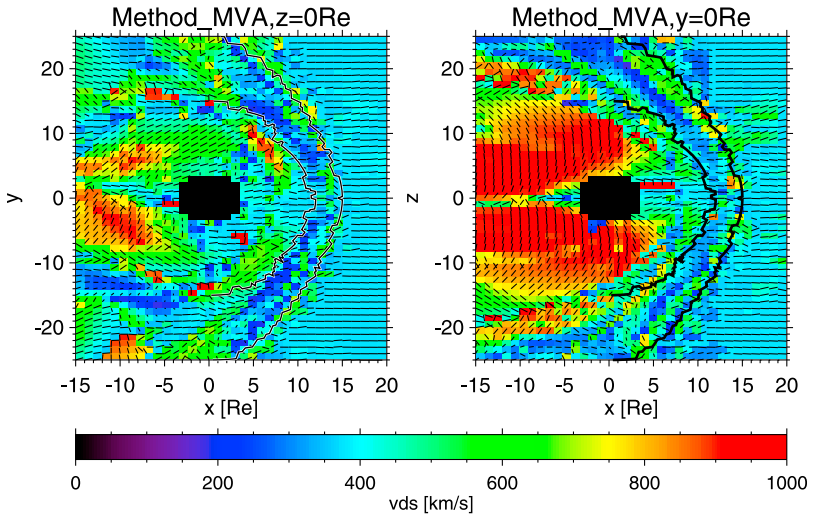

Figure 5. Shock/disturbance speed and direction in the solar wind/magnetosheath/magnetosphere, using MVA method. (left) Shock/disturbance speed (color coded) and propagation direction (lines) in the equatorial cross section. (right) Shock/disturbance speed (color coded) and propagation direction (lines) in the noon-midnight meridian plane. Lines represent shock/disturbance normal vectors to their fronts.

plane (Figure 5, right). Results, calculated from minimum variance analysis (MVA), are in good agreement with a previous observational study [see *Andréeová et al.*, 2008].

[25] Note that the plots in Figure 5 do not represent a single time step in the simulation. Rather, for each point in space, the shock speed and orientation is determined at the time when the disturbance first reaches that particular point (see Figure 4). In practice, for each point in the three-dimensional grid, we compute the time evolution of **v**, n, and **B** around the time of the shock arrival at that point. We then evaluate the disturbance direction using single spacecraft methods (VC, MC, MVA, RH), taking averaged values upstream and downstream of the discontinuity, and compute the normal direction. Using equation (2) we compute the impulse disturbance speed at each point. The final plot shows the pathways of the shock/disturbance in the two magnetospheric cut planes as the disturbance passes through the inner parts of the magnetosphere.

[26] While the background solar wind speed is about 320 km/s, the shock speed in the solar wind is about 360 km/s. In the magnetosheath the shock speed varies from 150 to 300 km/s. The disturbance speed inside the magnetosphere varies roughly from 350 to 1500 km/s. The disturbance speed increase at the shock is also clearly visible.

6. Ionospheric Observation Versus Magnetospheric Observation

[27] The fifth row in Figure 3 shows the field-aligned currents from the simulation. Figure 6 shows observation of ionospheric equivalent current density derived from the IMAGE magnetometer data with the 2-D SECS method [*Amm and Viljanen*, 1997; *Pulkkinen et al.*, 2003]. The equivalent current density is displayed by the black arrows. Current with a westward component has negative sign (blue color), current with a eastward component has positive sign (red color). Equivalent current was very weak before incoming shock related disturbance. At 1755 UT, a region of westward current intensified in the middle of the IMAGE region. At 1759 UT, a westward current weakened and disappeared at 1800 UT, observing only eastward current.

7. Discussion and Conclusion

[28] Fast forward shock (FFS) interacts with the Earth's bow shock, magnetosheath and magnetopause; after interaction with the FFS, the bow shock is modified and moves earthward. Shock front in the solar wind can be considered to be planar in the magnetospheric scale. In the magnetosheath the shock front becomes curved near the flanks in the magnetotail [*Koval et al.*, 2005, 2006a, 2006b]. The shock is decelerated after interaction with bow shock. Magnetopause starts to move earthward after interaction with the shock and launches different types of waves into the magnetosphere. Deceleration of the shock in the Earth's magnetosheath and acceleration of the impulse disturbance inside the magnetosphere in our study are in good agreement with previous studies [*Samsonov et al.*, 2006, 2007; *Yan and Lee*, 1996].

[29] Figures 2 and 3 show impulse disturbance propagation from different views. The line plots show tracing of the impulse disturbance from the solar wind toward the position of the Polar satellite. Density compression disappears near the terminator, but becomes again visible in the nightside. On the other hand, the magnetic field compression is visible at all x distances. In the nightside around -10 R_E, however, the compression changed rather into fluctuations in magnetic field when the background geomagnetic field becomes less than 15 nT.

[30] In the magnetosphere, the magnetic field disturbance propagates on one hand along the magnetopause, and on the other hand through the lobes and plasma sheet directly (Figure 3). The density disturbance propagates mostly along the magnetopause. For northward ($B_z > 0$) interplanetary magnetic field present in this event, four convection cells

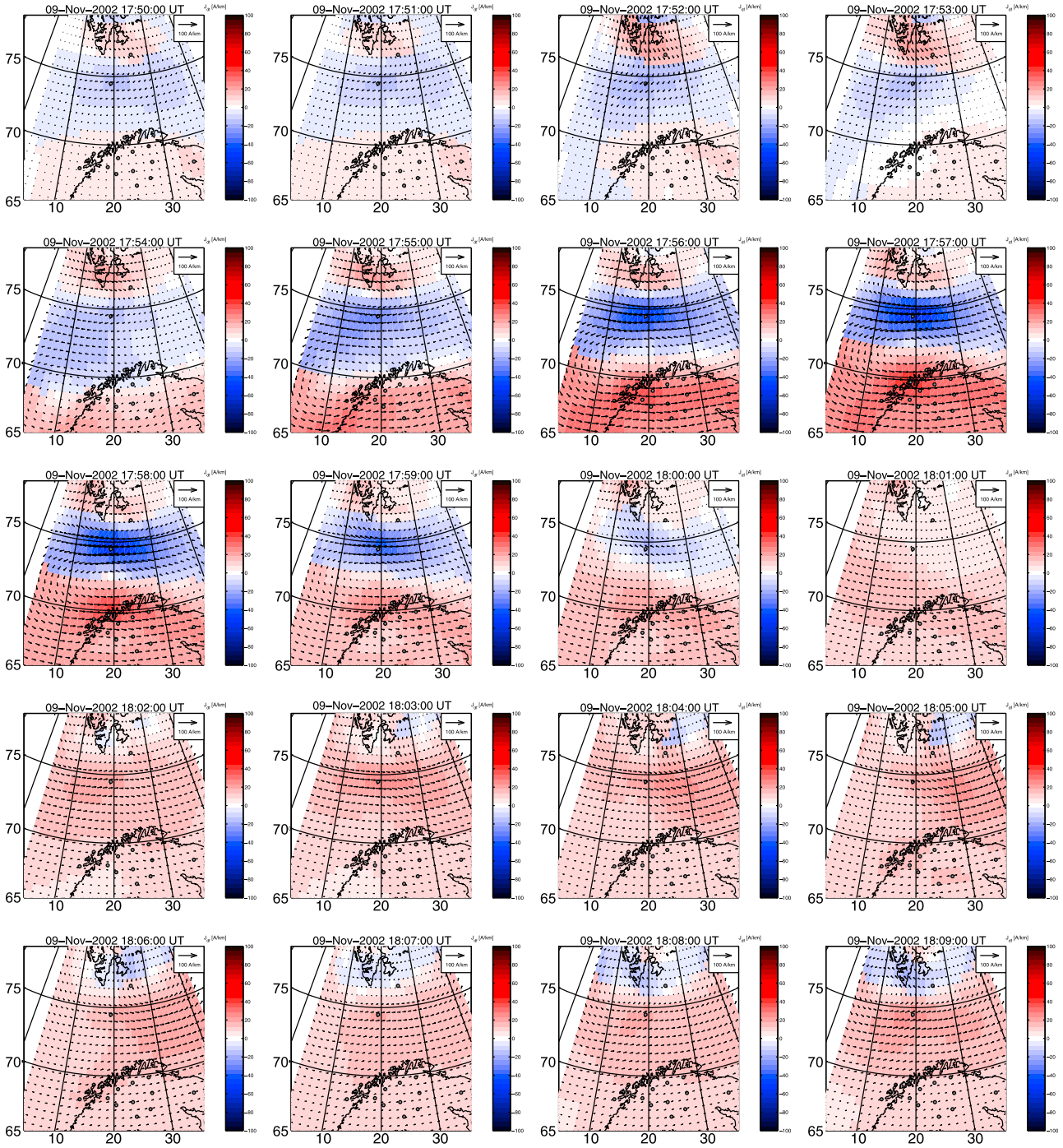

Figure 6. Ionospheric observation: field-aligned current density. Blue denotes westward direction of the flow, and red denotes eastward direction of the flow.

were intensified in the ionosphere (fifth row in Figure 3), driven by field-aligned currents that initiated the disturbance in the dayside ionosphere. This is in accordance with *Palmroth et al.* [2004, 2007], who found that the ionospheric currents intensify as a response to dynamic pressure changes in the solar wind.

[31] The shock/disturbance speeds of 450–1500 km/s discussed in this study and by *Andréeová and Přech* [2007] are consistent with earlier studies written by *Nopper et al.* [1982] and *Wilken et al.* [1982]. The impulse disturbance speeds in the magnetosphere are higher than the original shock speeds in the solar wind.

[32] In this study we observed weak reversal in equivalent current direction. Mapped to the magnetosphere, the eastward equivalent current would correspond to the antisunward plasma convection, and the westward equivalent current would correspond to the sunward plasma convection. In this region, plasma convection should be antisun-

ward. Convection was quite weak before incoming shock related disturbance because of weak and northward IMF (positive B_z), which was also observed by *Juusola et al.* [2010]. In our study [*Andréeová et al.*, 2008] we have observed double step-like structure in the dayside magnetosphere, observed by two satellites on both sites (dawn/dusk) GOES 8, and GOES 10. For this event we found a very steep initial part of the magnetic field compression in the GOES high-resolution data, with practically the same duration as the shock fronts in the solar wind (about 10 s), followed by a second much slower part. This double step-like structure lasted about 5 min. The first steep initial part would be related to the shock related disturbance, which may be followed by a reverse going wave, in the sense of the original direction of the shock related disturbance. Such reverse going wave is probably caused by the change in the direction of plasma convection. Duration and reverse going wave of this event is in good agreement with the ionospheric observation of equivalent current reversal after the shock related disturbance passage. Typically plasma should convect sunward. Such reversal of the direction of the convection could cause launching of the wave propagating with the opposite direction to the original direction of the shock related disturbance. Observing of second wave, related to reversal of the plasma convection, coincided with the second peak observed by GOES. Also, both signatures had their peak amplitude approximately at the same time, around 17:57.

[33] **Acknowledgments.** This work was supported by the Academy of Finland. We thank the CDAWeb service and the corresponding PIs for the satellite data. We thank the institutes who maintain the IMAGE Magnetometer Array.

[34] Philippa Browning thanks James Slavin and another reviewer for their assistance in evaluating this paper.

References

Abraham-Shrauner, B. (1972), Determination of magnetohydrodynamic shock normals, *J. Geophys. Res.*, *77*, 736–739.

Amm, O., and A. Viljanen (1997), Ionospheric elementary current systems in spherical coordinates and their application, *J. Geomagn. Geoelectr.*, *49*, 947–955.

Andréeová, K., and L. Přech (2007), Propagation of interplanetary shocks into the Earth's magnetosphere, *Adv. Space Res.*, *40*, 1871–1880, doi:10.1016/j.asr.2007.04.079.

Andréeová, K., T. I. Pulkkinen, T. V. Laitinen, and L. Přech (2008), Shock propagation in the magnetosphere: Observations and MHD simulations compared, *J. Geophys. Res.*, *113*, A09224, doi:10.1029/2008JA013350.

Berdichevsky, D. B., A. Szabo, R. P. Lepping, A. F. Vinas, and F. Mariani (2000), Interplanetary fast shocks and associated drivers observed through the 23rd solar minimum by Wind over its first 2.5 years, *J. Geophys. Res.*, *105*, 27,289–27,314.

Burlaga, L. F. (1971), Hydromagnetic waves and discontinuities in the solar wind, *Space Sci. Rev.*, *12*, 600–657.

Collier, M. R., J. A. Slavin, R. P. Lepping, K. Ogilvie, A. Szabo, H. Laakso, and S. Taguchi (1998), Multispacecraft observations of sudden impulses in the magnetotail caused by solar wind pressure discontinuities: Wind and IMP 8, *J. Geophys. Res.*, *103*, 17,293–17,306.

Grib, S. A. (1982), Interaction of non-perpendicular/parallel solar wind shock waves with the Earth's magnetosphere, *Space Sci. Rev.*, *32*, 43–48.

Grib, S. A., B. E. Briunelli, M. Dryer, and W.-W. Shen (1979), Interaction of interplanetary shock waves with the bow shock-magnetopause system, *J. Geophys. Res.*, *84*, 5907–5921.

Huttunen, K. E. J., J. Slavin, M. Collier, H. E. J. Koskinen, A. Szabo, E. Tanskanen, A. Balogh, E. Lucek, and H. Rème (2005), Cluster observations of sudden impulses in the magnetotail caused by interplanetary shocks and pressure increases, *Ann. Geophys.*, *23*, 609–624.

Janhunen, P. (1996), GUMICS-3: A global ionosphere-magnetosphere coupling simulation with high ionospheric resolution, in *Environment Modeling for Space-Based Applications*, edited by T.-D. Guyenne and A. Hilgers, *Eur. Space Agency Spec. Publ.*, *ESA SP-392*, 233–239.

Jeřáb, M., Z. Němeček, J. Šafránková, K. Jelínek, and J. Měrka (2005), A study of bow shock locations, *Planet. Space Sci.*, *53*, 85–94.

Juusola, L., K. Andréeová, O. Amm, K. Kauristie, S. E. Milan, M. Palmroth, and N. Partamies (2010), Effects of a solar wind dynamic pressure increase in the magnetospere and in the ionosphere, *Ann. Geophys.*, *28*, 1945–1959, doi:10.5194/angeo-28-1945-2010.

Koval, A., J. Šafránková, Z. Němeček, L. Přech, A. A. Samsonov, and J. D. Richardson (2005), Deformation of interplanetary shock fronts in the magnetosheath, *Geophys. Res. Lett.*, *32*, L15101, doi:10.1029/2005GL023009.

Koval, A., J. Šafránková, Z. Němeček, and L. Přech (2006a), Propagation of interplanetary shocks through the solar wind and magnetosheath, *Adv. Space Res.*, *38*, 552–558.

Koval, A., J. Šafránková, Z. Němeček, A. A. Samsonov, L. Přech, J. D. Richardson, and M. Hayosh (2006b), Interplanetary shock in the magnetosheath: Comparison of experimental data with MHD modeling, *Geophys. Res. Lett.*, *33*, L11102, doi:10.1029/2006GL025707.

Le, G., and C. T. Russell (1998), Initial polar magnetic field experiment observations of the low-altitude polar magnetosphere: Monitoring the ring current with polar orbiting spacecraft, *J. Geophys. Res.*, *103*, 17,345–17,350.

Le, G., C. T. Russell, and J. G. Luhmann (1998), POLAR magnetic observations of the low-altitude magnetosphere during the January 1997 coronal mass ejection/magnetic cloud event, *Geophys. Res. Lett.*, *25*, 2533–2536.

Lepping, R. P., and P. D. Argentiero (1971), Single spacecraft method of estimating shock normals, *J. Geophys. Res.*, *76*, 4349–4359.

Nopper, R. W., Jr., W. J. Hughes, C. G. Maclennan, and R. L. McPherron (1982), Impulse-excited pulsations during the July 29, 1977, event, *J. Geophys. Res.*, *87*, 5911–5916.

Palmroth, M., P. Janhunen, T. Pulkkinen, and H. Koskinen (2004), Ionospheric energy input as a function of solar wind parameters: Global MHD simulation results, *Ann. Geophys.*, *22*, 549–566.

Palmroth, M., N. Partamies, J. Polvi, T. I. Pulkkinen, D. J. McComas, R. J. Barnes, P. Stauning, C. W. Smith, H. J. Singer, and R. Vainio (2007), Solar wind-magnetosphere coupling efficiency for solar wind pressure impulses, *Geophys. Res. Lett.*, *34*, L11101, doi:10.1029/2006GL029059.

Paschmann, G., G. Haerendel, N. Sckopke, E. Moebius, and H. Luehr (1988), Three-dimensional plasma structures with anomalous flow directions near the Earth's bow shock, *J. Geophys. Res.*, *93*, 11,279–11,294.

Petrinec, S. M., and C. T. Russell (1996), Near-Earth magnetopause shape and size as determined from the magnetopase flaring angle, *J. Geophys. Res.*, *101*, 137–152.

Pulkkinen, A., O. Amm, and A. Viljanen (2003), Ionospheric equivalent current distributions determined with the method of spherical elementary current systems, *J. Geophys. Res.*, *108*(A2), 1053, doi:10.1029/2001JA005085.

Šafránková, J., Z. Němeček, L. Přech, A. A. Samsonov, A. Koval, and K. Andréeová (2007), Interaction of interplanetary shocks with the bow shock, *Planet. Space Sci.*, *55*, 2324–2329, doi:10.1016/j.pss.2007.05.012.

Samsonov, A. A., Z. Němeček, and J. Šafránková (2006), Numerical MHD modeling of propagation of interplanetary shock through the magnetosheath, *J. Geophys. Res.*, *111*, A08210, doi:10.1029/2005JA011537.

Samsonov, A. A., D. G. Sibeck, and J. Imber (2007), MHD simulation for the interaction of an interplanetary shock with the Earth's magnetosphere, *J. Geophys. Res.*, *112*, A12220, doi:10.1029/2007JA012627.

Spreiter, J. R., and S. S. Stahara (1994), Gasdynamic and magnetohydrodynamic modeling of the magnetosheath: A tutorial, *Adv. Space Res.*, *14*, 5–19.

Szabo, A. (1994), An improved solution to the "Rankine-Hugoniot" problem, *J. Geophys. Res.*, *99*(A8), 14,737–14,746, doi:10.1029/94JA00782.

Szabo, A., R. P. Lepping, J. Merka, C. W. Smith, and R. M. Skoug (2001), The evolution of interplanetary shocks driven by magnetic clouds, in *Solar Encounter. Proceedings of the First Solar Orbiter Workshop*, edited by B. Battrick et al., *Eur. Space Agency Spec. Publ.*, *ESA SP-493*, 383–387.

Tamao, T. (1964), The structure of three-dimensional hydromagnetic waves in a uniform cold plasma, *J. Geomagn. Geoelectr.*, *18*, 89–114.

Villante, U., S. Lepidi, P. Francia, and T. Bruno (2004), Some aspects of the interaction of interplanetary shocks with the Earth's magnetosphere: An estimate of the propagation time through the magnetosheath, *J. Atmos. Sol. Terr. Phys.*, *66*, 337–341.

Wilken, B., C. K. Goertz, D. N. Baker, P. R. Higbie, and T. A. Fritz (1982), The SSC on July 29, 1977 and its propagation within the magnetosphere, *J. Geophys. Res.*, *87*, 5901–5910.

Yan, M., and L. C. Lee (1996), Interaction of interplanetary shocks and rotational discontinuities with the Earth's bow shock, *J. Geophys. Res.*, *101*, 4835–4848.

Zhuang, H. C., C. T. Russell, E. J. Smith, and J. T. Gosling (1981), Three-dimensional interaction of interplanetary shock waves with the bow shock and magnetopause: A comparison of theory with ISEE observations, *J. Geophys. Res.*, *86*, 5590–5600.

K. Andreeova, Division of Geophysics and Astronomy, Department of Physics, University of Helsinki, PO Box 64, FI-00014 Helsinki, Finland. (katerina.andreeova@fmi.fi)

L. Juusola, M. Palmroth, and T. I. Pulkkinen, Finnish Meteorological Institute, Erik Palmenin aukio 1, FI-00560 Helsinki, Finland. (liisa.juusola@fmi.fi; minna.palmroth@fmi.fi; tuija.pulkkinen@fmi.fi)

O. Santolík, Institute of Atmospheric Physics AS CR, Bocni II/1401, 14131 Prague 4, Czech Republic.